Proceedings of the 2006 IEEE International Conference on Robotics and Automation
Orlando, Florida - May 2006

Analysis, Design and Control of a Planar Micro-robot Driven by Two Centripetal-Force Actuators*

Panagiotis Vartholomeos and Evangelos Papadopoulos
Department of Mechanical Engineering, National Technical University of Athens, 15780 Athens, Greece
barthol@central.ntua.gr, egpapado@central.ntua.gr

***Abstract* – This paper presents the motion analysis, design and position control of a novel, low cost, sliding micro-robot, which is actuated by centripetal forces generated by robot mounted vibration micro-motors. A new, two-micromotor design of the platform is presented, that improves system energy efficiency, and further does not necessitate for synchronous actuator operation and robot symmetry. The motion behavior of the micro-robot, for asynchronous actuation operation, is expressed analytically and simulation results are presented. A control strategy for microrobot x, θ_z position control that employs two motor speed controllers, and a platform position controller is designed. The control system performance is evaluated through the simulation of a successful trajectory tracking task. A prototype of the micro-robot has been constructed and is presented.**

Index Terms* – *Micro-positioning, micro-robot, feedback control

I. INTRODUCTION

Motion principles and actuation mechanisms that combine sub-micrometer motion of high resolution, and the speed virtues of coarse positioning, have been the subject of intensive studies in the last decade. Several micro-actuation techniques have been devised and are usually based on smart materials such as piezo-electric actuators, shape memory alloys, etc. The most popular micro-positioning motion mechanism is the stick-slip principle, which is implemented using piezoelectric actuators. This principle is employed by the 3DOF micro-robotic platform,[1], by the MINIMAN robot [2] and by the MiCRoN micro-robot, [3]. These platforms are capable of positioning accuracy of less than 200*nm,* and provide velocities of up to a few *mm/s*. The impact drive principle is employed by the 3 degrees of freedom (dof) micro-robotic platform Avalon, which provides step size of about 3.0 μm and speeds up to 1 *mm/s*, and is presented in [4]. A different motion mechanism based on piezo-tubes is utilized by the Nano Walker micro-robot presented in [5].
Although piezoelectric actuators seem to be the favored smart material for micro-positioning and do provide the required positioning resolution and actuation response, they usually suffer from complex power units that are expensive and cumbersome and which do not easily allow for untethered operation. Furthermore, piezoelectric actuators are complex systems that exhibit non-linear behavior and as a result they lack an accurate mathematical model that can provide a reliable prediction of the system's behavior. A novel and low-cost alternative approach is the six-axis nano-manipulator [6], based on a single-piece, flexible construction. Another interesting non-conventional motion principle employs inverse pendulum dynamics [7]. This paper presents an evolved micro robot design based on the concept proposed in [8,9]. It is a novel, simple and compact micro-robot that according to the theory [9] is able to perform translational and rotational sliding with sub-micrometer positioning accuracy and velocities up to $1.5mm/s$. All the components of the mechanism including its driving units, are of low cost and readily available. The motion mechanism is based on the interaction of centripetal forces generated by platform mounted vibrating micro-motors and friction forces at the base supports. The new design presented in this paper employs 2 micro-motors, instead of 3 in [8], resulting in a more stable and less power consuming actuation. This design does not necessitate for synchronous actuator operation, uniform mass distribution and in-phase motor operation, thus leading in an easily realizable motion principle. Analytical models of the platform, that incorporate non-symmetric inertial distribution and actuation non-uniformities, are derived and simulated. Actuator speed control is implemented using inverse dynamics and, platform position control for 2 dof is implemented by employing an external feedback loop and an appropriate control strategy. The performance of the controllers is evaluated through a simulated trajectory tracking task. A prototype of the micro-robot has been built and is demonstrated.

II. MOTION PRINCIPLE

The innovating actuation principle of the micro-robot is elaborated in [9]. What follows is a brief description of the physics that govern the motion principle. A simplified 1 dof mobile platform of mass M is used, whose motion mechanism employs an eccentric mass *m,* rotated by a platform mounted motor *O,* as shown in Fig. 1. One cycle of operation is completed when the mass has described an angle of 360^o.

* AKNOWLEDGEMENTS: This work is co-funded by the European Social Fund (75%) and National Resources (25%) - (EPEAEK II) – HRAKLEITOS.

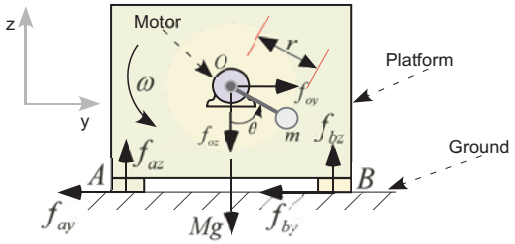

Fig. 1 Simplified 1dof platform with rotating mass m .

Gravitational and centripetal forces exerted on the rotating mass are resolved along the y-z axis to yield:

$$f_{oy} = mr\omega^2 \sin\theta$$
$$f_{oz} = -mg - mr\omega^2 \cos\theta \quad (1)$$

where g is the acceleration of gravity and r the length of the link between m and O. The equations of motion of the platform are derived in [8,9] and are numerically simulated to provide the results displayed in Fig. 2.

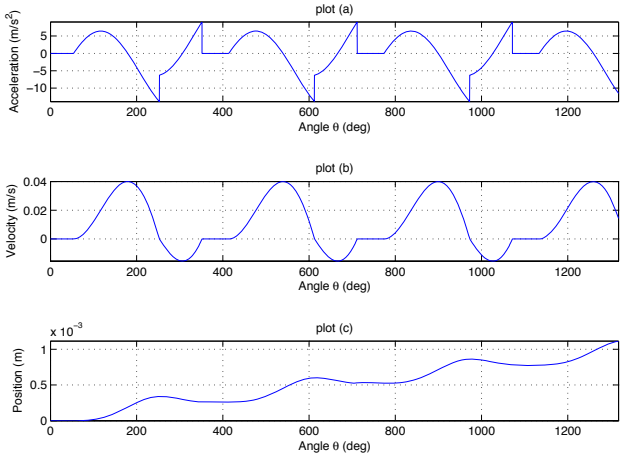

Fig. 2 Simulation results of the 1dof example.

From Figs. 2(a-c), it is clear that motion is induced. This occurs when the horizontal actuation force f_{oy} overcomes the static friction limit. Quite interestingly as shown in Fig. 2c, for a counterclockwise rotation of the motor, the platform exhibits a net displacement along the positive y-axis. This motion stems from the cyclic behavior of the actuation and friction forces applied on the platform and is explained next.

When the eccentric mass is at the lower points of its trajectory, the normal forces and therefore the frictional forces are high, whereas when the eccentric mass is at its highest points, the normal and frictional forces are low. Accordingly, for anticlockwise rotation of mass m initiated at $\theta = 0^\circ$, the platform tends not to move when m is at a low position and to move to the right when the mass is at high position. When m passes the highest point $\theta = 180^\circ$, the platform already has a non-zero velocity. As m moves past this point, friction forces together with actuation forces tend to decelerate the platform and even change its direction. As friction still increases eventually brings the platform to a stop. The actuation forces are now pointing to the left and as a result reverse platform motion is induced. Since the platform velocity became zero past the 180° point, there is less time for it to accelerate in the opposite direction and finally return back to its initial position before stopping again. Therefore, once a cycle is completed, the platform exhibits a net displacement as shown in Fig. 2c. Reversal of the direction of ω will lead to a reversal of the direction of motion. It should be pointed that the motion resolution of this actuation principle is not limited due to Stribeck friction, in fact if appropriate rotational speed ω is applied to the eccentric load m, then the forward displacement can be equal in magnitude to the reverse one, and consequently obtain zero net displacement.

III 2DOF PLANAR MOTION PLATFORM

The actuation principle mentioned above is employed to the design of a 2dof micro-robot. The design must meet a number of objectives for pertinent micro-positioning behavior, [8]. The first design attempt involved 3 actuators and allowed for 3dof planar motion [8,9]. However, through simulations and analytical investigation it was shown that when all 3 actuators operate, particular force components cancel each other resulting in zero work and thus reducing the robot efficiency. Moreover during 3dof motion, actuation coupling appears and the induced motion requires more sophisticated control algorithms. Hence, it was decided that the first prototypes should employ 2 actuators instead of 3, allowing only for local 2dof planar motion. This way operational simplicity and power efficiency are gained at the expense of 1 dof. The base of the 2dof design is shown in Fig. 3a.

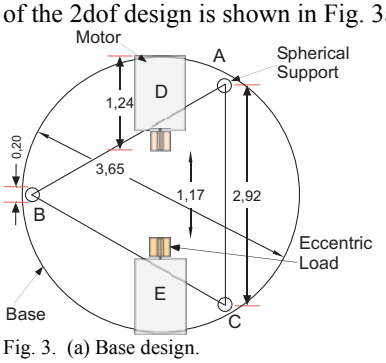

Fig. 3. (a) Base design.

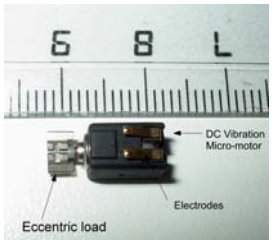

(b) Actuator.

The geometry of the base is a circular disk. The contact points (supports) A, B and C are arranged in an equilateral triangular order. No platform symmetry is assumed and thus the CM does not necessarily coincide with the geometrical center. The actuators (see Fig. 3b) are aligned on the diameter of the base and are directed opposite to each other. The eccentric loads are capable for bidirectional spin about the motor axis. The motion induced to the platform depends on the spin speeds of the actuators, the inertial distribution of the platform and the frictional distribution of the ground.

IV DYNAMIC ANALYSIS

The description of the dynamics of the micro-robotic platform requires the use of three dynamic models: First, the platform

dynamics, which are expressed through the corresponding equations of motion. Second, a mass-spring system that models the deformations of the platform base. Third, a dynamic model describing the response of the DC vibration micro-motor.

A. *Platform dynamics*

The only assumptions used for the platform dynamics are: (i) The imbalance load can be modelled as a point mass m , rotating at a distance r from the motor axis. (ii) The contact points of the platform experience Coulomb friction. No assumptions are made regarding the relative speed and phase of the actuators or the inertia distribution of the platform. The platform analysis involves the body-fixed frame {B,x,y} and the inertial frame {O,x,y} , see Fig. 4.

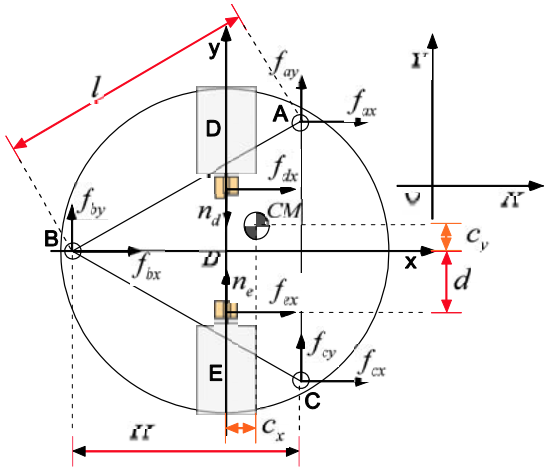

Fig. 4 Forces applied on the platform.

The adopted notation is ${}^{i}f_{j}$ where the superscript i is the frame index and subscript j is the component x, y, z index. The b superscript denotes frame B. Frame O uses no superscript. The position vectors of the contact points A, B and C are denoted by ${}^{b}\mathbf{r}_{a}, {}^{b}\mathbf{r}_{b}, {}^{b}\mathbf{r}_{c}$ and the position vectors of the motor axis points D and E on which the imbalance forces are applied are denoted by ${}^{b}\mathbf{r}_{d}, {}^{b}\mathbf{r}_{e}$. Forces ${}^{b}\mathbf{f}_{a}, {}^{b}\mathbf{f}_{b}, {}^{b}\mathbf{f}_{c}$ include the normal and frictional contact forces at contact points A, B and C, respectively. The angle θ, is the eccentric mass angle with respect to the vertical axis, see Fig. 1. Due to the rotating eccentricities, forces ${}^{b}\mathbf{f}_{d}, {}^{b}\mathbf{f}_{e}$, are applied at points D and E of the platform, and moments ${}^{b}\mathbf{n}_{d}, {}^{b}\mathbf{n}_{e}$ are applied about its motor axes, see Fig. 4. Their body-fixed components are given by,

$$
\begin{aligned}
{}^{b}f_{ix} &= -m_i r_i \omega_i^2 \sin\phi_i \sin\theta \\
{}^{b}f_{iy} &= 0 \\
{}^{b}f_{iz} &= -m_i g - m_i r_i \omega_i^2 \cos\theta \\
{}^{b}n_{ix} &= 0 \\
{}^{b}n_{iy} &= -m_i g r_i \sin\phi_i \sin\theta \\
{}^{b}n_{iz} &= 0
\end{aligned}
\qquad (2)
$$

where $i = \{d, e\}$, $\omega_i = \dot{\theta}_i$ is motor's i angular velocity, r_i is the eccentricity of the imbalance mass m_i and $\phi_i = \{90^\circ, -90^\circ\}$ are the angles of position vectors ${}^{b}\mathbf{r}_{d}, {}^{b}\mathbf{r}_{e}$. Then, the Newton-Euler equations of the platform are given by, [10]:

$$M\dot{\mathbf{v}} = \mathbf{R}\sum_{i} {}^{b}\mathbf{f}_{i}, \qquad i = \{a, b, c, d, e\} \qquad (3a)$$

$$
\begin{aligned}
&{}^{b}\mathbf{I}\dot{\boldsymbol{\omega}}_{p} + {}^{b}\boldsymbol{\omega}_{p} \times {}^{b}\mathbf{I}\,{}^{b}\boldsymbol{\omega}_{p} = \sum_{i}({}^{b}\mathbf{r}_{i} \times {}^{b}\mathbf{f}_{i}) + \sum_{i} {}^{b}\mathbf{n}_{j} \\
&i = \{a, b, c, d, e\},\ j = \{d, e\}
\end{aligned}
\qquad (3b)
$$

where $\mathbf{R}$ is the rotation matrix between frames B and O, $\boldsymbol{\omega}_{p}$ is the platform angular velocity, ${}^{b}\mathbf{I}$ is its inertia matrix, and $\mathbf{v} = [\dot{x}, \dot{y}, \dot{z}]^{T}$ is its CM position in the inertial frame. During analysis equations are simplified due to planar motion.

B. *Deformable body dynamics*

While the platform is static and the actuation forces gradually increase, the forces distributed to the platform legs reach the Coulomb level and motion is impending. It is required to have knowledge of the force distribution on each of the three supports A, B, and C of the triangular platform during static conditions. These six unknowns can be determined by considering small deformations along the base of the platform. For this purpose, the platform is modelled as a lumped system, consisting of three point masses connected via stiff springs as shown in Fig. 5.

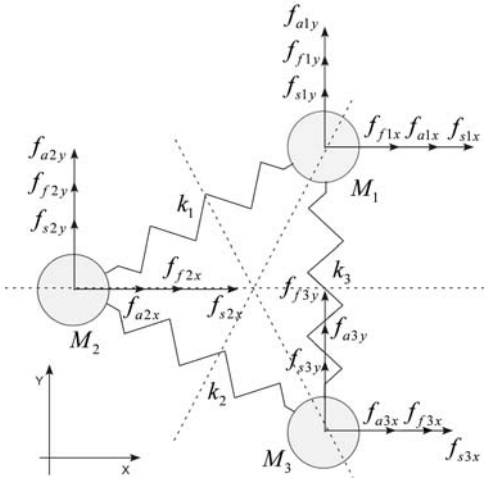

Fig. 5. Spring-Mass system of the base.

By solving the static equilibrium equations of the platform the vertical reactions at contact points A, B and C are found and consequently the lumped masses M_1, M_2, M_3 are calculated:

$$
\begin{aligned}
M_1 &= (2Hl(M + m_d + m_e) - 3lMc_x \\
&\quad -6H(Mc_y - (m_d - m_e)d))/(6Hl) \\
M_2 &= \frac{1}{3}(m_d + m_e + M + \frac{3Mc_x}{H}) \\
M_3 &= (2Hl(M + m_d + m_e) - 3lMc_x \\
&\quad +6H(Mc_y - (m_d - m_e)d))/(6Hl)
\end{aligned}
\qquad (4)
$$

Where l, H, d are dimensional parameters shown in Fig. 4 and (c_x, c_y) are the coordinates of the CM with respect to frame B. The constants k_1, k_2, k_3 represent the corresponding spring stiffness and m_d, m_e are the eccentric loads of motors D and E respectively. The produced deformations are adequately small so that the change in the angle of the springs is considered negligible. Forces $\mathbf{f}_{ai}, \mathbf{f}_{fi}, \mathbf{f}_{si}$ with $i = \{1,2,3\}$, are the actuation, friction and spring forces exerted at mass M_i. The dynamic equations of the spring-mass system are:

$$\begin{aligned} &\mathbf{M}\ddot{\mathbf{x}} = \mathbf{A}\mathbf{x} + \mathbf{f}_a + \mathbf{f}_f, \\ &\mathbf{x}(0) = \mathbf{0}, \dot{\mathbf{x}}(0) = \mathbf{0} \end{aligned} \tag{5}$$

where $\mathbf{M}$ is the mass matrix, $\mathbf{A}$ is a matrix containing spring constants, and $\mathbf{x} = [x_1, x_2, x_3, y_1, y_2, y_3]^T$ represents the x-y displacement of the three masses. When the masses are in a static state, the unknowns of the system are the six friction forces, which are determined by solving the six static equilibrium equations. When some or all of the masses are in motion, then the magnitude of the corresponding friction forces is determined by the Coulomb friction limit, whereas the direction of the friction forces is determined by the velocity of the corresponding mass.

C. Actuator dynamics

Actuators are modelled as systems comprising a DC permanent magnet motor and an imbalanced load. The input to the actuator is the voltage V_s. The dynamics of the actuator are expressed through the following equation,

$$\ddot{\theta} = -\frac{k_T^2}{RJ}\dot{\theta} - \frac{mgr}{J}\sin\theta - (\frac{c}{J}sign(\dot{\theta}) + \frac{b}{J}\dot{\theta}) + \frac{k_T}{RJ}V_s \tag{6}$$

where, k_T is motor's torque constant, R is its ohmic resistance, J is the inertia of the eccentric load, and the term $(\frac{c}{J}sign(\dot{\theta}) + \frac{b}{J}\dot{\theta})$ is the Coulomb and viscous friction.

V ASYNCHRONOUS ACTUATION

In the asynchronous case $\omega_d \neq \omega_e$, but the two frequencies have to be close to each other so that motion is induced, while at the same time hopping of the robots is avoided [9]. This means that the superposition of the actuation forces results to sinusoidal beats. The actuation force along the x dimension is given by:

$$\begin{aligned} &f_x(t) = A_d \sin(\omega_d t) - A_e \sin(\omega_e t) = |f_x(t)|\sin(\measuredangle f_x(t)), \\ &|f_x(t)| = \sqrt{A_d^2 + A_e^2 + 2A_d A_e \cos\{(\omega_e + \omega_d)t\}} \\ &\measuredangle f_x(t) = \tan^{-1}(\frac{A_d \sin\omega_d t - A_e \sin\omega_e t}{A_d \cos\omega_d t + A_e \cos\omega_e t}) \end{aligned} \tag{7}$$

where, $A_d = m_d r_d \omega_d^2, A_e = m_e r_e \omega_e^2$. Similarly, the z actuation force component is given by (8) and the actuation moment about z is given by (9).

$$\begin{aligned} f_z(t) &= -2mg - (A_d \cos(\omega_d t) + A_e \cos(\omega_e t)) \\ &= -2mg + |g_z(t)|\cos(\measuredangle g_z(t) + \pi), \end{aligned} \tag{8}$$

$$\begin{aligned} &|g_z(t)| = \sqrt{A_d^2 + A_e^2 + 2A_d A_e \cos((\omega_d + \omega_e)t)} \\ &\measuredangle g_z(t) = \tan^{-1}(\frac{A_d \sin\omega_d t - A_e \sin\omega_e t}{A_d \cos\omega_d t + A_e \cos\omega_e t}) \\ &M_z(t) = -(s_d A_d \sin(\omega_d t) + s_e A_e \sin(\omega_e t)) \\ &= |M_z(t)|\sin(\measuredangle M_z(t) + \pi), \\ &|M_z(t)| = \{(s_d A_d)^2 + (s_e A_e)^2 + \\ &2s_d s_e A_d A_e \cos((\omega_d + \omega_e)t + \pi)\}^{1/2} \\ &\measuredangle M_z(t) = \tan^{-1}(\frac{s_d A_d \sin\omega_d t + s_e A_e \sin\omega_e t}{s_d A_d \cos\omega_d t - s_e A_e \cos\omega_e t}) \end{aligned} \tag{9}$$

Where, s_d, s_e are the distances of loads m_d, m_e from CM. The actuation magnitude is modulated by an envelop function, which is periodic with period $P_b = 2\pi/(\omega_d + \omega_e)$. The frequency of the resulting actuation signal lies somewhere between the two initial frequencies (ω_d, ω_e) and varies periodically with period P_b. Table I presents the relative phase between the three actuation signals as this can be calculated by (6-9). The phase of the carrier signals are given approximately.

Table I. Relative phases of the three actuation forces.

Signal	$f_x(t)$	$f_z(t)$	$M_z(t)$
Envelop	$(\omega_d + \omega_e)t$	$(\omega_d + \omega_e)t$	$(\omega_d + \omega_e)t + \pi$
Carrier	$\frac{(\omega_d - \omega_e)t}{2}$	$\frac{(\omega_d - \omega_e)t}{2} + \frac{\pi}{2}$	$\frac{(\omega_d - \omega_e)t}{2} - \frac{\pi}{2}$

The force $f_z(t)$ and hence the vertical reactions at the contact points of the platform are almost in phase with $f_z(t)$. This means, that the friction forces are also in phase with $f_z(t)$. As stated in section I, the actuation forces interact with the friction forces and yield a net planar displacement. Phase difference between $f_z(t)$ and $f_x(t)$ or $M_z(t)$ affects the direction of motion and the magnitude of the motion step. Considerable displacement per step, in the desired direction, is induced when the horizontal actuation forces (or moments) are 180° to 90° out of phase with respect to the vertical reactions. This means (see Table I), that this platform may exhibit both linear and rotational displacement. If the actuation signals have a relative phase difference ϕ, then this angle is incorporated into (6-9) and the sinusoidal beat gets shifted by an angle ϕ. This phase shift does not affect the motion principle, meaning that the actuators may have any relative phase difference when they initiate spinning. The beat behaviour of the signals leads to displacements that are composed by an alternating sequence, of static and motion regions that correspond to the valleys and peaks of the modulated magnitude of the actuation forces.

The following simulation demonstrates the robot behaviour when the actuation forces operate asynchronously. The

simulated robot's mass is non-uniformly distributed. The CM is located at $(c_x, c_y) = (2,2)mm$ and actuation speeds are set to $(\omega_d, \omega_e) = (1200, -1050) rad/s$. Figure 6 depicts the actuation forces $f_x(t)$, $f_z(t)$ and $M_z(t)$. Figure 7 demonstrates the resulting displacement.

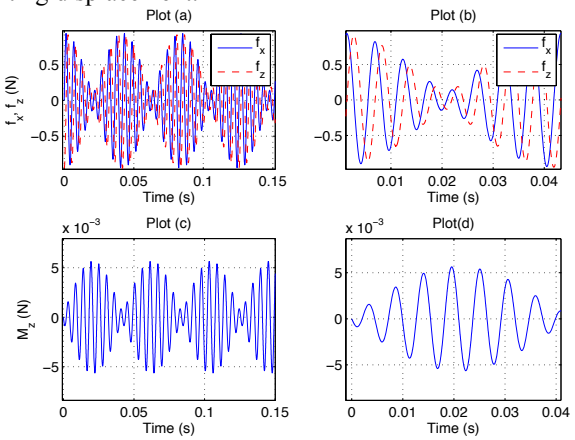

Fig. 6. Sinusoidal beat actuation, plots (b,d) are zoom in on plots (a,c).

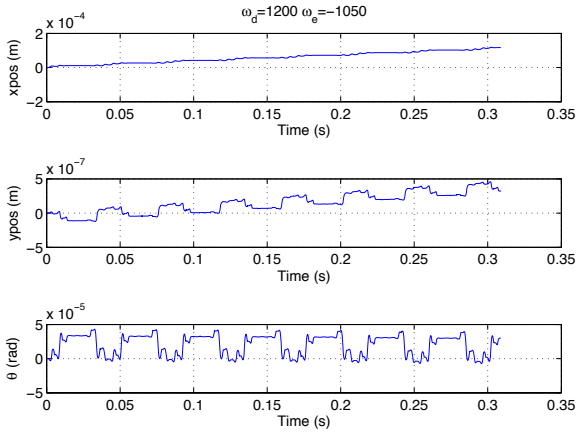

Fig. 7 Trajectories for asynchronous actuation.

The robot CM is located towards the leg A, hence due to the vertical reaction distribution it was expected that platform would exhibit a positive rotation about leg A. Interestingly this is not observed, because the actuation moment counteracts the moments caused by the uneven friction forces. The example suggests that by driving appropriately the two actuators, the x and θ dofs can be both controlled. By exploiting these two dofs the platform may move on the x-y plane, from any initial configuration to any final one [11]. To this aim, closed loop control is employed and simulated in the following paragraph.

VI Closed Loop Control

The control system employs a nested loop architecture. It comprises an inner motor speed controller for each motor and an outer robot position controller.

A Motor speed control

The platform almost rapidly acquires the velocity imposed by the actuators (within 1 cycle of operation). It is expected that an improvement of the actuators speed response will result to an analogous improvement to the platform's velocity response. To this aim, the motor is controlled using inverse dynamics plus a 2nd order control law u given by (10):

$$V_s = \{(k_t^2 + Rb)\omega + Rmgr\sin(\omega t) + cR\}k_t^{-1} + d + u$$
$$u = K_P(\omega - \omega_{ref}) + K_I\int(\omega - \omega_{ref})dt \quad (10)$$

The controller is schematically presented in Fig. 8. The inverse dynamics linearize (6). The terms K_p, K_I eliminate the steady state error of the motor's speed and result to a much faster response. A disturbance d has been added to model systematic errors of the inverse dynamics.

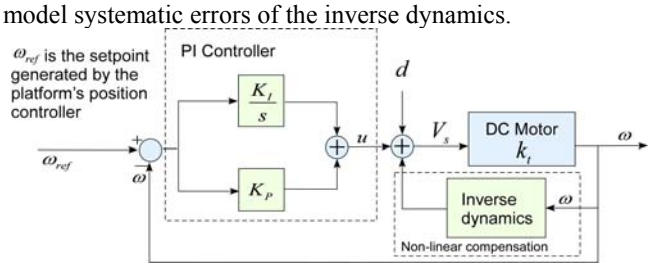

Fig. 8. Motor controller.

B Robot position control

The goal is to control the body-fixed x and θ dofs. A schematic diagram of the control loop is depicted in Fig. 9. The position controller is expressed by (11).

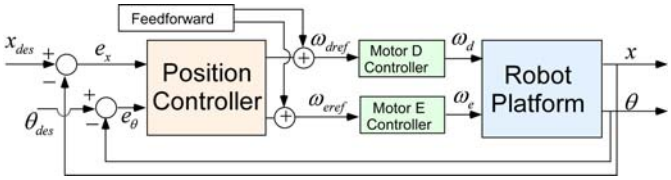

Fig. 9 Control system of the micro-robot.

$$\begin{bmatrix}\dot{\omega}_d \\ \dot{\omega}_e\end{bmatrix} = \begin{bmatrix}k_x & -k_{\theta d} \\ -k_x & -k_{\theta e}\end{bmatrix}\begin{bmatrix}e_x \\ e_\theta\end{bmatrix} \quad (11)$$

The position error e_x is processed by a P controller with equal gains k_x for motor D and E. The angle error e_θ is also processed by a P controller whose gains $k_{\theta d}, k_{\theta e}$ vary depending on the sign of the angle θ. A feedforward term of ω_{ref} is computed for each motor, using the dynamic analysis and is added to the output of the position controller to ensure that motors work within the operating region.

The control system performance is evaluated through a simulation example. The platform performs: (i) tracking of the body-fixed x_{des} trajectory and (ii) regulation of the angle $\theta_{des} = 0$. The trajectory of x is generated using a second order blended polynomials time law, [10]. Analytical results and open loop simulations suggest that reasonable values for the cruise velocity of the micro-robot and t final are

$\dot{q}_c = 1.510^{-2} m/s$ and $t_f = 0.9s$. The desired and actual trajectories are demonstrated on Fig. 10.

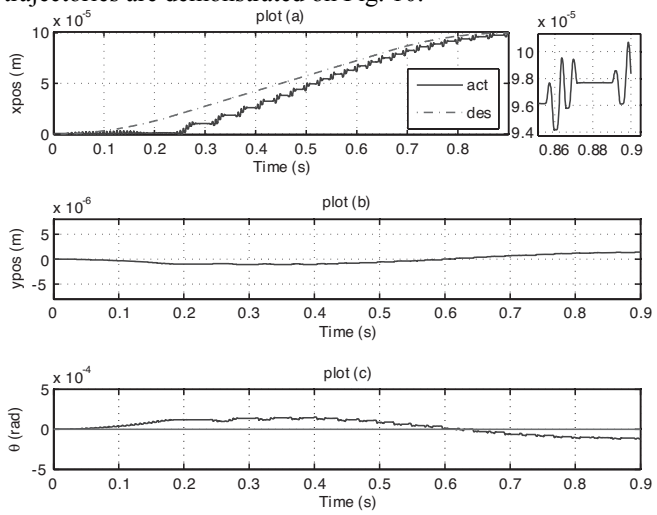

Fig. 10. Trajectory tracking results.

Plot (a) indicates that the controller performs successful tracking and covers approximately 100 μm (ignoring the y-displacement). The zoom-in of plot (a) depicts typical motion steps. The static and motion regions due to the sinusoidal beat actuation are also clear. Plot (c) demonstrates the bounded angle error ($\pm 1 \cdot 10^{-5} rad$).

VII Implementation

Using the analytical equations derived in section IV, design guidelines are derived which lead to the selection of the design parameters of Table II. The first prototype is built, see Fig. 11a and 11b. The base is made of a cylindrical solid piece of plexiglass within which, the two actuators have been integrated. At the top of the base, a stack of removable weights have been securely placed, so that the robots mass can vary according to the required speed range. At the top of the weights two PCB discs are placed for hosting of processing power and driving circuits.

Table II Design parameters

Parameter	Value	Parameter	Value
R	0.00177 [m]	l	0.03 [m]
M	0.00021[kg]	h_o	0.004 [m]
M	0.12 [kg]	μ	0.4

Fig. 11 (a) Lateral view of the robot.

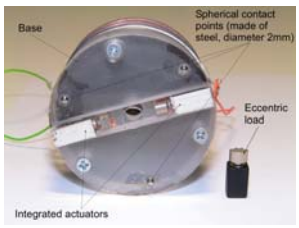

(b) Base with integrated actuators.

Currently the robot is powered by a single battery of 1.2V. Preliminary experiments have demonstrated that the robot is capable for maximum translational speeds within the range of $0.5-1.5mm/s$, depending on the (variable) mass of the platform. An interferometric sensor is been assembled by the authors, for conducting experiments with micrometric and sub-micrometric displacement accuracy.

VIII Conclusions

The paper presented the analysis and design of a novel micro-robotic platform, employing two vibration micro-motors. The micro-robot is able to perform translational and rotational sliding with sub-micrometer accuracy and develop velocities up to 1.5 mm/s. Dynamic analysis of the robots motion was presented. The new design does not necessitate for synchronous actuator operation, uniform mass distribution and in-phase motor operation. Platform's 2dof planar motion capabilities under asynchronous actuation were examined using analysis and simulations. A nested control architecture, which comprises an inner motor speed controller and an outer robot position controller, was designed. The system's performance was evaluated through the simulation of a trajectory tracking task. A prototype has been built according to the analysis presented in this paper. Preliminary results have shown translational speeds up to 1.5mm/s, as predicted.

References

[1] Jean-Marc Breguet, Reymond Clavel, Stick and Slip Actuators: design, control, performances and applications. International Symposium on Micromechatronics and Human Science (MHS), (Nagoya), 1998, 89-95.

[2] F. Schmoeckel, S. Fatikow, Smart Flexible Microrobots for Scanning Electron Microscope (SEM) Applications. SPIE's 7th Int. Symp. On Smart Structures and Materials: Integrated systems, Newport Beach, California, USA, 5-9 March 2000.

[3] J. Brufau, M. Puig-Vidal, et. al, MICRON: Small Autonomous Robot for Cell Manipulation Applications, Proc. of the IEEE International Conference on Robotics & Automation, Barcelona, Spain, April 18-22, 2005.

[4] Roland Büchi, Wolfgang Zesch, Alain Codourey, Inertial Drives for Micro- and Nanorobots: Analytical Study. Proc. of SPIE Photonics East '95: Microrobotics and Micromachanical Systems Symp, Vol. 2593, Philadelphia, PA, Lynne E. Parker - Bellingham, WA, SPIE, 1995.

[5] Martel Sylvain et al., THREE-LEGGED WIRELESS MINIATURE ROBOTS FOR MASS-SCALE OPERATIONS AT THE SUB-ATOMIC SCALE. Proc. of the 2001 IEEE International Conference on Robotics & Automation, Seoul, Korea, May 21-26, 2001.

[6] "Nanomanipulator", MIT Technology Review, Oct. 2004, pp. 80-84.

[7] Lida, Fumiya Raja, D. and Chandana, R., "Design and control of a pendulum driven hopping robot," *Proc. 2002 IEEE/RSJ International Conference on Intelligent Robots and Systems*, v3, 2002,. pp. 2141-2146.

[8] P. Vartholomeos, E. Papadopoulos. "Analysis and Design of a Novel Mini-platform Employing Vibration Micro-motors," Proc. of the 2005 IEEE International Conference on Robotics & Automation, Barcelona, Spain, April 18-22, 2005.

[9] P. Vartholomeos, E. Papadopoulos. "Dynamics Design and Simulation of a Novel Micro-robotic Platform Employing Vibration Micro-actuators", Journal of Dynamic Systems, Measurement and Control, in press.

[10] L.Sciavicco and B. Siciliano, Modelling and Control of Robot Manipulators, Springer-Verlag London Ltd, 2001.

[11] G. Wilforng, "Motion Planning for an Autonomous Vehicle", Proc. Int. Conf. Automation., 1988 pp. 529-533.